engineering proceedings

MDPI

Proceeding Paper

Impact of Current Variations on Weld Bead Properties During the Cold Metal Transfer (CMT) Welding of 7075 Aluminium Using an ER4043 Filler Wire †

Vishal Bhardwaj *, Siddharth Garg and Qasim Murtaza

Department of Mechanical Engineering, Delhi Technological University, Delhi 110042, India; officialsiddharthgarg@gmail.com (S.G.); qasimmurtaza@dce.ac.in (Q.M.)

* Correspondence: itsmevishal1234@gmail.com

† Presented at the International Conference on Mechanical Engineering Design (ICMechD 2024), Chennai, India, 21–22 March 2024.

Abstract

This study investigated into how different current input levels during cold metal transfer (CMT) welding affected the characteristics of the weld bead. For the current variation, three input values were taken: 80 A, 90 A, and 100 A. Weld beads fabricated from all three current inputs were compared by analysing their microstructure, microhardness, tensile strength, and residual stress. The microhardness of the weld bead decreased when the current parameter was increased from 80 A to 100 A. The average tensile strength increased from 80 A to 90 A. The lowest residual stress calculated was −135 MPa with 100 A current.

Keywords: CMT welding; Aluminium-7075; tensile; microhardness; residual stress

check for updates

Academic Editors: M. S. Alphin, Divya Zindani, M. Nalla Mohammed and Ramkumar P.

Published: 1 August 2025

Citation: Bhardwaj, V.; Garg, S.; Murtaza, Q. Impact of Current Variations on Weld Bead Properties During the Cold Metal Transfer (CMT) Welding of 7075 Aluminium Using an ER4043 Filler Wire. *Eng. Proc.* **2025**, *93*, 22. https://doi.org/10.3390/engproc2025093022

Copyright: © 2025 by the authors. Licensee MDPI, Basel, Switzerland. This article is an open access article distributed under the terms and conditions of the Creative Commons Attribution (CC BY) license (https://creativecommons.org/licenses/by/4.0/).

1. Introduction

Currently, aluminium is utilised in place of steel in a number of industries, including shipbuilding, aerospace, and the manufacture of boilers, body panels for automobiles, and internal and external body panels. Its light weight, which drastically lowers the vehicle's energy consumption and transportation costs, is the primary element driving aluminium's acceptance over steel [1]. Moreover, aluminium and its alloys are also known for their high strength and excellent corrosion resistance. Al-Zn alloys, commonly known as the 7xxx series, are predominantly used in the aerospace industry due to their superior strength (over 500 MPa) [2]. Moreover, there has been a recent surge in research and applications concerning the use of 7xxx alloys, particularly 7075, in automobile parts. This alloy, renowned as the primary choice for aircraft components owing to its exceptional strength, exhibits an ultimate tensile strength ranging from 510 to 540 MPa and maintains a mean hardness of 140 $HV_{0.5}$. This combination of strength and hardness makes 7075 aluminium alloys highly desirable for demanding applications in automotive engineering [3].

On the other hand, 4000 series alloys are commonly employed as filler materials in welding and brazing due to their minimal susceptibility and excellent fluidity at lower heat inputs, and mostly outperform other aluminium alloy series in terms of strength and porosity [4]. Among the 4000 series aluminium alloys, ER4043 (with a tensile strength of 206 MPa) is a popular Al-Si alloy used as a filler material because of its greater fluidity and reduced tendency to develop faults in welded joints [5].

Based on the conventional short-circuiting transfer technology created by 'Fronius of Austria', cold metal transfer (CMT) is an enhanced method of gas metal arc welding

(GMAW) [6]. During CMT welding, one-quarter of the entire duration will be spent in a short-circuit phase when the current amplitude is nearly nil. This cuts utilised energy and welding costs up to 40% [7]. This approach differs from GMAW's conventional short-circuiting (CSC) approach. Liquid droplet separation from the filler wire is the primary distinction between CSC and CMT. Droplet detachment in CSC is caused by Lorentz forces, whereas the CMT principle of wire retraction motion has been proposed [8]. Due to its shallow non-zero current, CMT welding can effectively join thin sheets without causing deformation due to minimal thermal heat input [9]. CMT may be used to fuse extremely thin sheets such as aluminium foil (0.3 mm) [10]. It has a significant gap bridging capacity while maintaining a spatter-free weld.

In addition to the weld materials and welding process, the welding parameters mainly affect weld quality. Many factors impact weld quality, such as the voltage (V), current (I), speed of welding (S), wire feed rate (WFR), stick-out distance, rate of flow of the shielding gas, and contact tip-to-workpiece distance (CTWD). In previously carried-out works, current variation was shown to be the most significant contributor to the variation in weld quality produced using CMT welding; thus, in the following experiments, the current was varied, which simultaneously changed the voltage and wire feed rate, and for each current input, the microstructure, microhardness, and residual stress were investigated. A suitable range of 80 A to 100 A was identified through the available literature and experimental testing; going above that range leads to the production of holes, whereas going below leads to significantly weak joints being produced.

2. Experimental Methods and Materials

In this experiment, thin sheets of Al 7075 were joined with ER4043 (AlSi5%) filler wire with a diameter of 1.2 mm. The dimensions of the substrate used were 100 mm × 150 mm × 3 mm. The substrates were placed in a butt joint configuration with zero distance between them. Table 1 shows the metallurgical composition of the base material and the filler wire material calculated through optical emission spectroscopy (OES). The experiment was conducted using a Fronius TPS 400i CMT machine (Fronius International, Pettenbach, Austria) (shown in Figure 1a). The contact tip to work distance (CTWD) was set to 5 mm for better penetration. A schematic diagram of the welding fixtures employed in the joining process is shown in Figure 1b. For the fabrication of the samples, three current inputs were considered—80 A, 90 A, and 100 A—while the other welding parameters were kept constant, because of which the current input is directly correlated with the amount of heat input; please refer to Table 2. An Olympus microscope was used for microstructural analysis. The 2 cm × 2 cm welded samples were epoxy-mounted and then polished in a stepwise manner using emery papers with grit sizes ranging from 400 to 2500. The polished samples were then placed on the microscope for examination after undergoing a 30 s etching procedure in Keller's reagent (2.5% HNO3, 1% HF, 1.5% HCl, and distilled water). Microhardness analysis was performed using the Duramin-40 M1 Vickers microhardness testing machine (Struers, New Delhi, India) with a constant load of 100 g and a 10 s dwell time following the ASTM E384 standard [11]. The ASTM E8 standard was used for tensile specimen formation using a CNC machine (Mtab Engineers Pvt. Ltd., Chennai, India). The tensile strength test was carried out on a Tinius Olsen UTM (Tinius Olsen India Private Limited, Uttar Pradesh, India) with a ram speed of 1 mm/min [12]. The residual stresses of the samples were obtained using a Pulstec μ-X360n Full 2D X-ray system (Pulstec Industrial Co., Ltd., Hamamatsu, Japan) (Japan). Since X-ray diffraction (XRD) has a limited penetration depth (usually approximately 10 μm), it was adopted as the main methodology for measuring near-surface residual stress. The samples were exposed to radiation at a voltage of 30 kV and a beam current of 0.66 mA, all within carefully calibrated parameters.

The X-ray beam incidence angle was purposefully adjusted to 30°, which increased the measurement accuracy. The cos α method, which is fundamental to the μ-X360 X-ray Pulstec system, serves as the basis for computing in-plane residual stress [13].

Table 1. Metallurgical composition (wt. %) of the substrate material and filler wire.

Material	Al	Cu	Zn	Si	Mg	Fe	Mn	Cr	Ti
Al 7075	**90.2**	**1.2**	**5.1**	**0.4**	**1.9**	**0.5**	**0.3**	**0.2**	**0.2**
ER4043	**93.03**	**0.3**	**0.1**	**5.6**	**0.05**	**0.8**	**0.05**	**0.05**	**0.02**

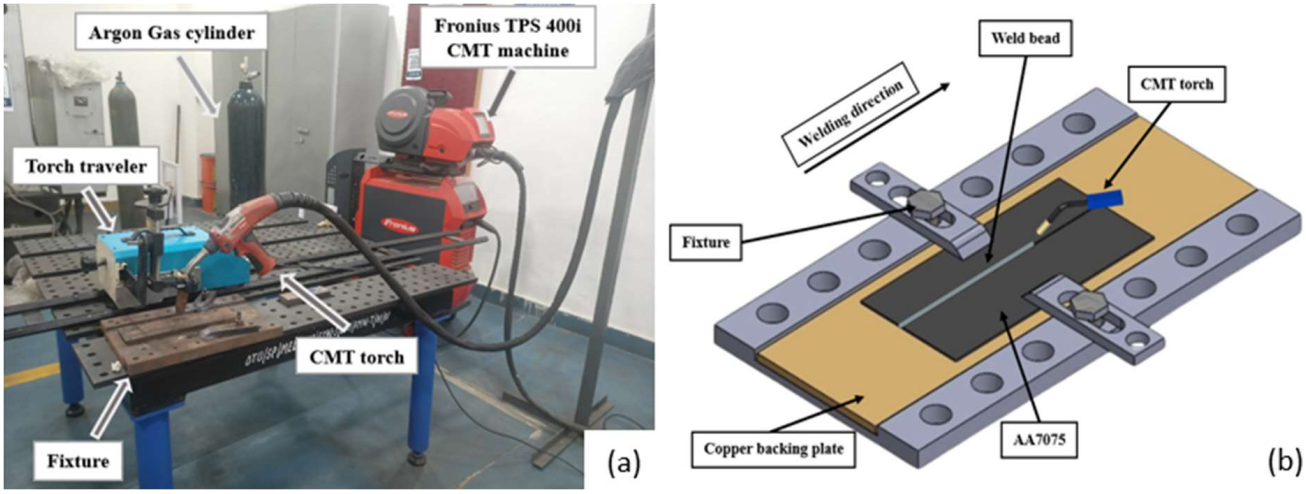


Figure 1. (**a**) Experimental setup for the CMT machine. (**b**) Schematic diagram of fixtures used along with weld configuration.

Table 2. Welding parameters.

Current (A)	Voltage (V)	Wire Feed Rate (m/min)	Time (s)	Length (mm)	Gas Flow Rate (L/min)	Heat Input (kJ)
80	**14**	**4.80**	**10**	**100**	**15**	**0.102**
90	**14.8**	**4.89**	**10**	**100**	**15**	**0.121**
100	**15.5**	**5.10**	**10**	**100**	**15**	**0.143**

3. Microstructural Analysis

The microstructural images depicted in Figure 2 reveal equiaxed dendrite formations within the weld bead. These dendrites exhibit a noticeable increase in size as the welding current escalates from 80 A to 100 A, attributed to the amplified heat input with higher current settings [14]. This phenomenon directly correlates the dendrite size augmentation with the intensified thermal energy. Figure 3 demonstrates the microstructure of the heat-affected zone (HAZ), displaying coarse grain structures. Particularly intriguing is the observation that at 80 A current input, the base metal (BM) and the HAZ share a similar grain structure, but with increasing current, the disparity in grain size between the HAZ and BM becomes more pronounced. This disparity underscores the sensitivity of grain structure to welding parameters, notably current intensity, and its consequent impact on microstructural characteristics within the welded region.

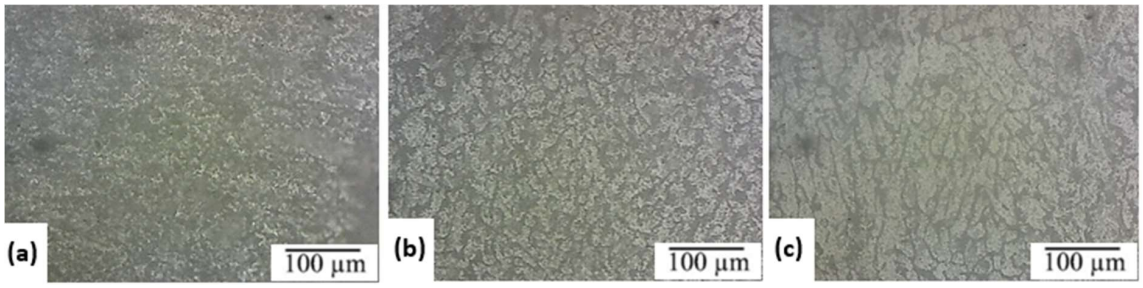


Figure 2. Microstructural image of the weld bead at 500× (100 µm) at (**a**) 80 A, (**b**) 90 A, and (**c**) 100 A.

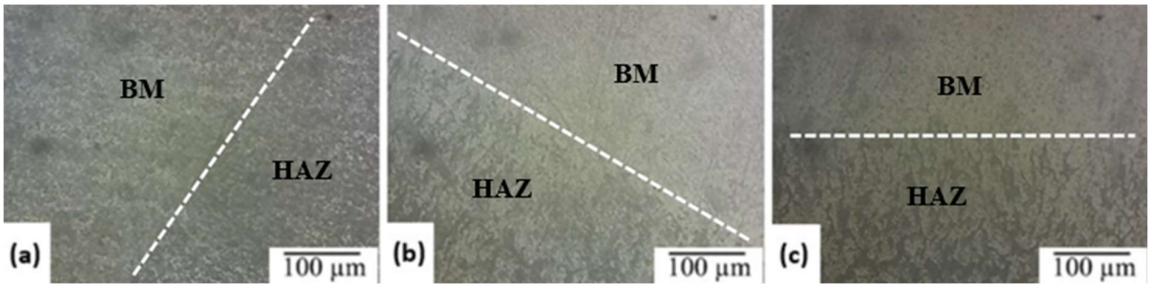


Figure 3. Microstructural image of the heat-affected region near the fusion zone at 500× (100 µm) at (**a**) 80 A, (**b**) 90 A, and (**c**) 100 A.

4. Microhardness Analysis

Microhardness was measured from the left end with a 0.1 mm gap before the starting point and further increased with a 1 mm gap for the rest of the readings [15]. Figure 4 shows the microhardness of the cross section with varying input currents, from which it can be seen that the range for the 80 A weld bead is 85–125 $HV_{0.1}$, that for the 90 A weld bead is 90–135 $HV_{0.1}$, and that for the 100 A weld bead is 80–122 $HV_{0.1}$. The weld metal (WM) had the lowest microhardness of 79 $HV_{0.1}$ at the highest current input of 100 A and the highest microhardness of 91 $HV_{0.1}$ at the lowest current input of 80 A. Further, a decline in microhardness from the BM to the HAZ is notable for all three specimens. This variation can be attributed to various factors, such as alloying elements, grain size, and precipitate volume fraction, on which the hardness of the WM depends. The strengthening elements magnesium and zinc evaporate during the welding process in the WM, significantly decreasing the hardness of the base metals used for fabricating the joint [16]. Moreover, grain coarsening also decreases the microhardness of the WM. Moving from the WM to the HAZ and further to the BM, the hardness increases as the amount of alloying elements (such as Zn and Mg) and grain size gradually come to their original state (less exposed to heat) [17].

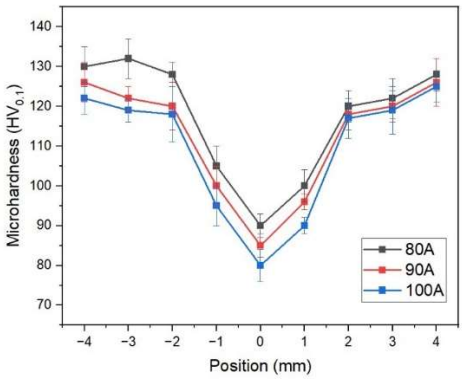


Figure 4. Microhardness trend for varying current speeds in CMT-welded samples.

5. Effect of Current on Tensile Strength

The ASTM E8 method was followed to prepare four tensile samples for each current parameter. The average tensile strength and percentage elongation of each current parameter weld are shown in Table 3. As the current increased from 80 A to 90 A, a slight increase in the tensile strength was observed (Figure 5), while the elongation of the specimen decreased from 9.5% to 8%. The increase in strength was because of the satisfactory fusion of the weld metal with the base metal, while at a current of 100 A, the strength decreased because of grain coarsening due to increased heat input, which caused the specimen to fracture earlier, resulting in an elongation percentage of 6.5% [18]. The decreasing value of elongation reflects the brittleness of the joint and coarse grain formation. The fractography of the specimens with currents of 80 A, 90 A, and 100 A is shown in Figure 6. The specimens first displayed a ductile mode of failure at low current input; however, as the current increased, the mode of failure approached brittle fracture. As the current increased from 80 A to 100 A, the size of the dimples increased, accompanied by the formation of large voids, which ultimately reduced the joint strength. The presence of fine equiaxed dimples indicates the ductile nature of fracture while the presence of interstitial voids and flat planes in the fractured surface reveals the brittle nature of the fracture [19].

Table 3. The average tensile strength and elongation according to their current parameters.

Current (A)	Average Tensile Strength (MPa)	Elongation (%)
80	420	9.5
90	450	8
100	400	6.5

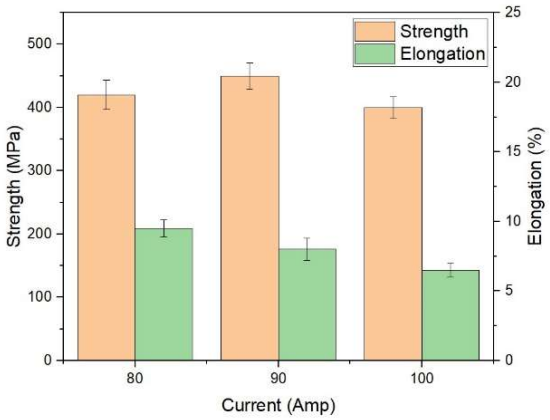


Figure 5. Average tensile strength and percentage elongation achieved for CMT-welded samples.

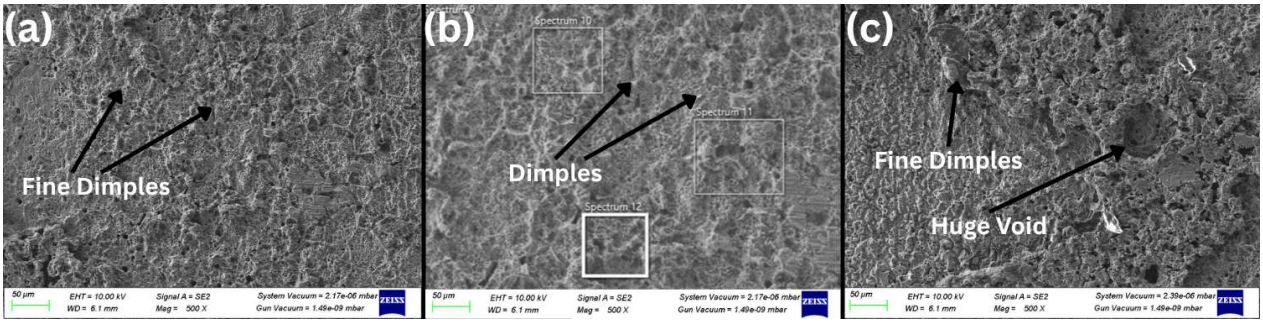


Figure 6. Fracture surface of samples with current parameters of (**a**) 80 A, (**b**) 90 A, and (**c**) 100 A.

6. Residual Stress Analysis

Residual stress measurements were systematically taken at six specific positions along the vertical axis of the welded sample. These residual stress values depend on multiple factors, such as the weld geometry, deposited weld metal, weld bead size, total deposited weld volume, and cooling rate [20]. As shown in Figure 7, a residual stress dip can be observed for the 80 A, 90 A, and 100 A beads in the fusion zone (FZ). The dip in the fusion weld zone depicts a higher compressive stress than that of the weld and base metal. The reason behind this difference was the higher heat input and faster cooling rate than those of the weld bead and base metal, respectively. A compressive residual stress is favourable for improving the fatigue behaviour of welds. Base plate distortion and crack propagation are caused by residual stress, which increases as the current level and welding speed decrease. Thus, to increase the fatigue behaviour of joined parts, compressive residual stresses are purposefully created, and various techniques, including spot heating, post-weld heat treatment, and shot peening are used in an attempt to minimise residual tensile stresses.

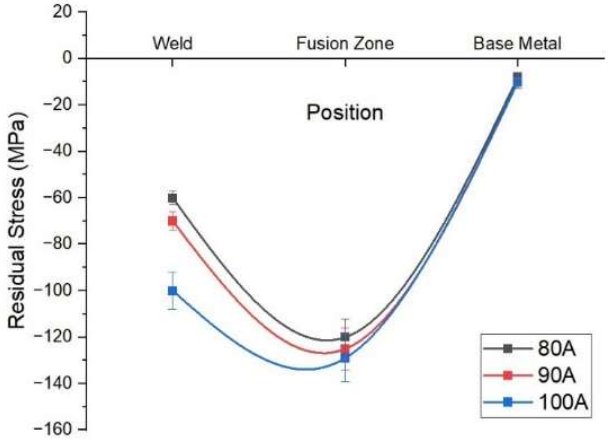


Figure 7. Residual stress for CMT-welded samples.

7. Conclusions

Following an in-depth analysis of specific experimental investigations carried out by changing the current input parameters from 80 A to 100 A, the following conclusions were drawn:

1. The microstructural investigation revealed that as the current input increased, the grain size also increased in the HAZ and bead region.
2. When the current input increased from 80 A to 100 A, the hardness decreased in the WM. The reason behind this increase was the increase in grain size due to the high heat input.
3. The average tensile strength exhibited by the 90 A current samples reached a maximum (450 MPa). This was because of the satisfactory fusion of the weld metal with the base metal.
4. The calculated residual stress decreased as the current parameter increased, reaching its lowest value at −135 MPa with 100 A current; this is explained by the weld's increased heat input and quicker cooling rate.
5. Ultimately, it was determined that when using the ER4043 filler wire to fabricate Al 7075, the 90 A weld bead produced the best results.

Author Contributions: All the authors contributed to the study conceptualisation and design. Material preparation, experimentation, analysis, and the writing of the first draft of the manuscript were performed by V.B. Analysis, the writing of the first draft of the manuscript, and subsequent

editing were carried out by S.G. Q.M. contributed to the study supervision and manuscript writing. All authors have read and agreed to the published version of the manuscript.

Funding: This research received no external funding.

Institutional Review Board Statement: Not applicable.

Informed Consent Statement: Not applicable.

Data Availability Statement: The original contributions presented in this study are included in the article. Further inquiries can be directed to the corresponding authors.

Acknowledgments: We would like to express our sincere gratitude to Delhi Technological University for providing the cold metal transfer welding machine, which was integral to the success of this research.

Conflicts of Interest: The authors declare no conflicts of interest.

References

1. Hayat, F. Electron Beam Welding of 7075 Aluminum Alloy: Microstructure and Fracture Properties. *Eng. Sci. Technol. Int. J.* **2022**, *34*, 101093. [CrossRef]
2. Ion, J.C. Laser Beam Welding of Wrought Aluminium Alloys. *Sci. Technol. Weld. Join.* **2000**, *5*, 265–276. [CrossRef]
3. Hirsch, J. Recent Development in Aluminium for Automotive Applications. *Trans. Nonferrous Met. Soc. China* **2014**, *24*, 1995–2002. [CrossRef]
4. Vimal, K.E.K.; Naveen Srinivas, M.; Rajak, S. Wire Arc Additive Manufacturing of Aluminium Alloys: A Review. *Mater. Today Proc.* **2021**, *41*, 1139–1145. [CrossRef]
5. Izan, N.; Hussein, S.; Ket, G.C.; Rahim, A.; Ayof, M.N.; Zaimi, M.; Abidin, Z.; Srithorn, J. Process and Heat Resources for Wire Arc Additive Manufacturing of Aluminium Alloy ER4043: A Review. *J. Mech. Eng.* **2023**, *20*, 21–41. [CrossRef]
6. Nandan, G.; Arora, K.S.; Singh, J.; Kumar, A. Influence of Process Parameters on Bead Geometry and Its Effect on Mechanical Properties of CMT Welding of Automotive Grade Steel and Aluminium Alloy Using Aluminium Based Filler Wire. *Weld. Int.* **2023**, *37*, 493–506. [CrossRef]
7. Bhardwaj, V.; Singh, I.J.; Murtaza, Q. Progressive Developments in Cold Metal Transfer Welding Technique: A Review and Trends. *J. Polym. Compos.* **2024**. Available online: https://journals.stmjournals.com/jopc/article=2024/view=137975/ (accessed on 2 April 2024).
8. Bellamkonda, P.N.; Sudersanan, M.; Visvalingam, B. A Study on Tensile Properties and Microstructural Characteristics of Wire Arc Additive Manufactured Low Carbon Steel Cylindrical Components. *Weld. Int.* **2022**, *36*, 443–454. [CrossRef]
9. İrizalp, A.O.; Durmuş, H.; Yüksel, N.; Türkmen, İ. Cold Metal Transfer Welding of AA1050 Aluminum Thin Sheets. *Rev. Mater.* **2016**, *21*, 615–622. [CrossRef]
10. Kannan, R.A.; Shanmugam, N.S.; Naveenkumar, S. Effect of Arc Length Correction on Weld Bead Geometry and Mechanical Properties of AISI 316L Weldments by Cold Metal Transfer (CMT) Process. *Mater. Today Proc.* **2019**, *18*, 3916–3921. [CrossRef]
11. Garg, S.; Bansal, S.; Murtaza, Q. Failure Investigation of an Elbow Pipe Used in Sewage Water Treatment Facility. *Mater. Corros.* **2024**, *75*, 1185–1192. [CrossRef]
12. Garg, S.; Murtaza, Q. Effect of Filler Paste's Mixing Ratio on the Properties of Al-64430 Dip-Brazed Joints. *Weld. World* **2024**, *68*, 2459–2471. [CrossRef]
13. Chauhan, G.; Sahu, M.; Prasad, P.; Bhattacharya, S.; Ganguly, S. Evolution of Residual Stresses in Friction Stir Welded Joints of AA7039. *J. Inst. Eng. (India) Ser. D* **2023**, *104*, 213–223. [CrossRef]
14. Babu, S.; Panigrahi, S.K.; Janaki Ram, G.D.; Venkitakrishnan, P.V.; Suresh Kumar, R. Cold Metal Transfer Welding of Aluminium Alloy AA 2219 to Austenitic Stainless Steel AISI 321. *J. Mater. Process Technol.* **2019**, *266*, 155–164. [CrossRef]
15. Garg, S.; Murtaza, Q. Comparative Analysis of Dip-Brazing and TIG Welding on the Properties of Al-64430 Joints. *J. Adhes. Sci. Technol.* **2024**, *39*, 386–400. [CrossRef]
16. Wu, S.; Yu, X.; Zuo, R.; Zhang, W.; Xie, H.; Jiang, J. Porosity, Element Loss, and Strength Model on Softening Behavior of Hybrid Laser Arc Welded Al-Zn-Mg-Cu Alloy with Synchrotron Radiation Analysis. *Weld. J.* **2013**, *92*, 64–71.
17. Masumura, R.A.; Hazzledine, P.M.; Pande, C.S. Yield Stress of Fine Grained Materials. *Acta Mater.* **1998**, *46*, 4527–4534. [CrossRef]
18. Koli, Y.; Yuvaraj, N.; Aravindan, S. Vipin Enhancement of Mechanical Properties of 6061/6082 Dissimilar Aluminium Alloys Through Ultrasonic-Assisted Cold Metal Transfer Welding. *Arab. J. Sci. Eng.* **2021**, *46*, 12089–12104. [CrossRef]

19. Pramod, R.; Shanmugam, N.S.; Krishnadasan, C.K. Studies on Cold Metal Transfer Welding of Aluminium Alloy 6061-T6 Using ER 4043. *Proc. Inst. Mech. Eng. Part L J. Mater. Des. Appl.* **2020**, *234*, 924–937. [CrossRef]
20. Koli, Y.; Yuvaraj, N.; Vipin; Aravindan, S. Investigations on Weld Bead Geometry and Microstructure in CMT, MIG Pulse Synergic and MIG Welding of AA6061-T6. *Mater. Res. Express* **2019**, *6*, 1265e5. [CrossRef]

Disclaimer/Publisher's Note: The statements, opinions and data contained in all publications are solely those of the individual author(s) and contributor(s) and not of MDPI and/or the editor(s). MDPI and/or the editor(s) disclaim responsibility for any injury to people or property resulting from any ideas, methods, instructions or products referred to in the content.